Nonlinear dynamics and conformational changes of linear entangled polymers using the Rolie-Poly model with an “effective” maximum contour length

Kabanemi, Kalonji; Hétu, Jean-Francois

Publisher’s version / Version de l'éditeur:

Rheologica Acta, 2009-07-03

Rheol Acta
DOI 10.1007/s00397-009-0373-9

ORIGINAL CONTRIBUTION

Nonlinear dynamics and conformational changes of linear entangled polymers using the Rolie-Poly model with an "effective" maximum contour length

Kalonji K. Kabanemi · Jean-François Hétu

Received: 14 January 2009 / Accepted: 10 June 2009

Abstract The extended Rouse-CCR tube model for linear entangled polymers recently proposed by the authors (Kabanemi and Hétu, J Non Newtonian-Fluid Mech 160:113–121, 2009), designed to capture the progressive changes in the average internal structure (kinked state) of polymer chains, is here used to analyze, by means of a time-dependent three-dimensional finite element method, chain segment dynamics, pressure drop, and stability of flow through a 4:1:4 constriction in a tube. The model predicts an enhancement of the pressure drop in the stretch-dominated flow regime, which is also observed experimentally. This excess pressure drop was not associated with the onset of flow instability. The model also predicts kinked configurations within chain segments in the entry section to the constriction tube, at the inception of flow, and prior to the development of upstream vortices. It is also shown how these kinked configurations within chain segments influence pressure drop transients.

Keywords Tube model · Viscoelastic fluid · Extensional flow · Entry flow · Entanglement

Introduction

There is continuing interest in obtaining a fundamental understanding of the rheological properties of dilute and entangled polymer solutions. Thanks to huge amount of experimental studies on entry flows of viscoelastic fluids, especially by Boger et al. (1986), Lawler et al. (1986), McKinley et al. (1991), Cartalos and Piau (1992), Rothstein and McKinley (1999) and Nigen and Walters (2002), among others, a rich store of knowledge on the behavior of polymer solutions in complex flows has been accumulated. Despite considerable efforts, many fundamental questions regarding mechanisms of the enhancement in the pressure drop and flow transitions in these polymer systems remain unresolved.

As far as dilute solutions are concerned, the experimental results by Lawler et al. (1986) for the flow of the low concentration PIB Boger fluid through an abrupt axisymmetric contraction have revealed a transition to a three-dimensional, time-dependent flow at a small Deborah number, $De_1 = 0.8$, prior to the development of large, upstream vortices. At larger Deborah number, $De_2 = 1.2$, they observed a sudden disappearance of the time-dependent motion and a reestablishment of a two-dimensional, steady flow. More than one time-dependent flow was detected between De_1 and De_2. McKinley et al. (1991) observed a similar Hopf bifurcation with a different PIB Boger fluid. In sharp contrast with the experimental results by Lawler et al., the flow remained time-dependent for all Deborah numbers greater than De_2 and subsequently underwent a series of nonlinear transitions. Cartalos and Piau (1992) studied the creeping flow regimes of low concentration polymer solutions in thick solvents through an orifice die. Their visualizations showed that small-scale instabilities throughout the converging zone do exist under conditions where the upstream flow may seem to possess a mean stable axisymmetric structure, at relatively low pressures. Once they appear, these instabilities are present in all higher subsequent

K. K. Kabanemi (✉) · J.-F. Hétu
Industrial Materials Institute (IMI), National Research Council of Canada (NRC), 75 de Mortagne, Boucherville, Québec, Canada J4B 6Y4
e-mail: kalonji.kabanemi@cnrc-nrc.gc.ca

Published online: 01 July 2009

regimes. They also observed three particular modes of pressure drop variation with flow rate: the initial linear (viscous) regime, the intermediate quadratic (elastic) regime, and the ultimate linear (viscous) regime. More recently, Rothstein and McKinley (1999, 2001) discussed, in depth, the role of the extensional rheology on vortex growth dynamics and the enhanced pressure drop during flow of a polystyrene Boger fluid through axisymmetric contraction–expansion geometry. They also analyzed the role of the extensional rheology in the differences in flow transitions for fluids with identical shear properties. As Cartalos and Piau, they observed that the enhancement in the pressure drop was not associated with the onset of flow instability. They conjectured that this extra pressure drop is the result of an additional dissipative contribution to the polymeric stress arising from stress-conformation hysteresis in strong nonhomogeneous extensional flow near contraction plane. Such a stress-conformation hysteresis was observed and computed by Doyle et al. (1998) and Li and Larson (2000) in transient uniaxial extensional flow, using Brownian dynamics simulations of bead-spring model.

In the case of entangled silicone fluids, Piau et al. (1988, 1990) provided additional information about the role of elongational properties, elasticity and shear thinning, on the appearance and the expansion of lip vortices. They also determined the Weissenberg number threshold from which the axisymmetric flow becomes unstable, but the exact mechanism of the upstream flow instability is still unknown. On the other hand, much less is known about the stress-conformation hysteresis in strong flows of entangled polymer solutions than their dilute solutions counterpart. The stress and birefringence growth of a concentrated entangled polystyrene solution (PS12) in uniaxial extensional flows has been recently documented by Rothstein and McKinley (2002). Contrary to the dilute polystyrene solution, they observed a less pronounced stress-conformation hysteresis during imposed stretching and subsequent stress relaxation at a strain rate of about, $\dot{\varepsilon}_0 = 5.3\ \mathrm{s}^{-1}$.

It is therefore useful to focus effort on the definition of suitable and numerically tractable rheological models that could reproduce, at least, qualitatively all the important flow features in the different flow regimes and, eventually, capture the onset of real physical instabilities occurring in these complex flows. In this spirit, Kabanemi and Hétu (2009) recently extended the Rouse-CCR tube model for linear entangled polymers (Rolie-Poly equation), developed by Likhtman and Graham (2003), by incorporating the concept of "effective" maximum contour length of polymer chains, to capture progressive changes in the average internal structure (kinked state) of chain segments. The rheological behavior of the model was favorably compared with various results already published in the literature for the entangled polystyrene solutions. It was shown that the extended Rolie-Poly model, with an "effective" maximum contour length, exhibits a less pronounced hysteretic behavior in stress versus birefringence in start-up of uniaxial extensional flow and subsequent relaxation, compared to that of a dilute polystyrene solution. Only simple shear and uniaxial extensional flows were scrutinized in that study.

The primary purpose of this work is to analyze the behavior of the extended Rolie-Poly model in a mixed complex flow, with the objective of capturing all the important flow features in different flow regimes. For the sake of clarity, we find it useful to briefly recall the basic physics of the extended Rolie-Poly model as developed by Kabanemi and Hétu. We then examine the ability of a fully three-dimensional time-dependent finite element method for calculating flow transitions or Hopf bifurcations in complex flow problems without periodic boundary conditions. An alternative to this approach would be to perform a linear or a weakly nonlinear stability analysis. In order to address complex flows, we use an approach that combines the matrix-logarithm-based formulation of the conformation tensor as proposed by Fattal and Kupferman (2004), the stabilized discrete elastic viscous stress splitting method (DEVSS; Guénette and Fortin 1995), the streamline upwind Petrov–Galerkin technique (SUPG) as developed by Carew et al. (1993), and the stabilized Galerkin least-squares method (GLS; Ilinca et al. 2000; Bonvin et al. 2001). Finally, we conclude by demonstrating the ability of the model in predicting the enhancement of the pressure drop and the kinked state of polymer chains in a constriction flow.

Rolie-Poly model with finite extensibility

We shall consider a constitutive model, called Rolie-Poly equation, standing for Rouse linear entangled polymers (Likhtman and Graham 2003). The model was derived from a molecular theory (Graham et al. 2003) that does not need decoupling approximation, which leads to averages for orientation tensor and chain stretching. In this model, the conformation of the polymer chain, $\boldsymbol{\sigma}$, in a flow field, $\boldsymbol{u}$, evolves in time by an equation of the form

$$\dot{\boldsymbol{\sigma}} = \boldsymbol{L} \cdot \boldsymbol{\sigma} + \boldsymbol{\sigma} \cdot \boldsymbol{L}^T + \boldsymbol{f}(\boldsymbol{\sigma}) \tag{1}$$

where the tensor function, $\boldsymbol{f}$, for a non-Gaussian chain with finite extensibility included, is given by

$$\boldsymbol{f}(\boldsymbol{\sigma}) = -\frac{1}{\tau_d}(\boldsymbol{\sigma} - \boldsymbol{I}) - \frac{2}{\tau_R} k_s(\lambda)\left(1 - \sqrt{\frac{3}{tr\boldsymbol{\sigma}}}\right)\left(\boldsymbol{\sigma} + \beta\left(\frac{tr\boldsymbol{\sigma}}{3}\right)^{\delta}(\boldsymbol{\sigma} - \boldsymbol{I})\right). \tag{2}$$

Here, $\boldsymbol{L} = \nabla \boldsymbol{u}^T$ is the transpose of velocity gradient tensor; τ_d is the fixed-tube disengagement time or reptation time; τ_R is the longest Rouse time or stretch time; β is the CCR coefficient analogous to the coefficient introduced by Marrucci in his original CCR paper (Marrucci 1996); δ is a negative power which can be obtained by fitting to the full theory; $\boldsymbol{\sigma} = \boldsymbol{I}$ is the equilibrium value of the conformation tensor in the absence of flow; $k_s(\lambda)$ is the nonlinearity of the spring coefficient accounting for the finite extensibility of polymer chains, equals unity for linear springs, and becomes much greater than unity as the spring becomes nearly fully stretched; and $\lambda = \sqrt{tr\boldsymbol{\sigma}/3}$ is the chain stretch ratio, and $\lambda = 1$ is its equilibrium value in the absence of flow.

The nonlinear spring coefficient, $k_s(\lambda)$, is approximated by the normalized Padé inverse Langevin function (Pattamaprom et al. 2000), i.e.,

$$k_s(\lambda) = \frac{\left(3 - \lambda^2/\lambda_{max}^2\right)\left(1 - 1/\lambda_{max}^2\right)}{\left(1 - \lambda^2/\lambda_{max}^2\right)\left(3 - 1/\lambda_{max}^2\right)}, \tag{3}$$

where λ_{max} is the fixed maximum stretch ratio.

The constitutive equation, Eq. 1, with the expression for the tensor function, $\boldsymbol{f}$, given by Eq. 2, is completed by specifying the relationship between the polymeric stress contribution $\boldsymbol{\tau}_p$ and the conformation tensor $\boldsymbol{\sigma}$. For a non-Gaussian chain, $\boldsymbol{\tau}_p$ is taken to be of the form

$$\boldsymbol{\tau}_p = Gk_s(\lambda)(\boldsymbol{\sigma} - \boldsymbol{I}) = \frac{\eta_p}{\tau_d} k_s(\lambda)(\boldsymbol{\sigma} - \boldsymbol{I}), \tag{4}$$

where G is the plateau modulus and η_p is the zero-shear-rate polymer viscosity.

Extended Rolie-Poly model with an effective maximum contour length

The extended Rolie-Poly model, recently proposed by Kabanemi and Hétu (2009), designed to capture the progressive changes in the average internal structure, i.e., kinked state and elongated coil within a single chain segment, is now considered. We shall here only briefly recall the basic physics of the model and refer the reader to the literature cited above. In rapidly changing flows, the dynamics of the average quantity, $\boldsymbol{\sigma}$, as described by Eq. 1, with the expression for the tensor function, $\boldsymbol{f}$, given by Eq. 2, using the inverse Langevin force law, does not lead to accurate descriptions of changes in polymer chain configuration on significantly shorter-length scales. Indeed, the inverse Langevin force law, obtained from equilibrium statistical mechanics, should be used with caution in nonequilibrium situations, in which the unfolding process of polymer chains takes place under nonequilibrium conditions.

Before proceeding, let us recall that the maximum length to which a tube segment can be stretched is given by $l_{max} = 0.82 n_e b_0$ (or equivalently, $\lambda_{max} = l_{max}/l_0$), where n_e is the number of backbone bonds in an entanglement spacing, b_0 the backbone bond length, and l_0 the equilibrium tube segment length. We would like to emphasize here that the pre-factor 0.82 and not 1 enters because the backbone has a zigzag configuration in the most extended state that still preserves the tetrahedral backbone bond angle restrictions (Ye et al. 2003). Since the kinked state seems to impede the molecular stretching, it is reasonable to assume that the coexistence of kinked conformations and elongated coil within a single chain segment reduces its flexibility and results in a shorter maximum length that we call here "apparent" or "effective" maximum length, l_{eff}, to which a tube segment can be stretched.

Let us now consider the situation where the polymer chain is stretched at a strain rate exceeding its reciprocal Rouse time τ_R, and let us suppose that the polymer chain does not have the opportunity to fully relax the imposed deformation at each stage of stretching via reptation, retraction, or CCR. Under these conditions, each chain segment will not have sufficient time to fully sample its configuration space. We, therefore, put forward the idea that kinked conformations and elongated coil will coexist within a single chain segment and will reduce its flexibility along with its maximum extensibility. In other words, only a fraction of the maximum contour length, l_{max}, of the chain segment, identified by, l_{eff}, will be equilibrated at each stage of stretching; otherwise, the chain segment would be able to fully sample its configuration space at each stage of deformation. As a consequence, the chain segment is forced to stretch with a shorter effective maximum contour length, l_{eff} (or equivalently, $\lambda_{eff} = l_{eff}/l_0$), compared to the original fixed maximum contour length, l_{max}. On average, this description, based on the effective

maximum contour length, represents a coarse-grained approximation of internal conformation states (kinked conformations and elongated coil) of a chain segment during rapid stretching. If we identify this chain segment with a non-Gaussian chain having a maximum contour length ratio, λ_{eff}, then the nonlinear spring coefficient, obtained from equilibrium statistical mechanics, approximated by the normalized Padé inverse Langevin function, Eq. 3, can be used equivalently. Then the spring coefficient becomes

$$k_s(\lambda) = \frac{\left(3 - \lambda^2/\lambda_{\text{eff}}^2\right)\left(1 - 1/\lambda_{\text{eff}}^2\right)}{\left(1 - \lambda^2/\lambda_{\text{eff}}^2\right)\left(3 - 1/\lambda_{\text{eff}}^2\right)}. \tag{5}$$

Then, the next step is to calculate the effective maximum contour length ratio, λ_{eff}, under a given condition.

More specifically, in strong extensional flows, for which $\dot{\varepsilon}\tau_{\text{R}} > 1$, polymer chains are significantly stretched, and the instantaneous rate of stretch is bounded, at each stage of stretching, by

$$0 \leq \left|\frac{d\lambda}{dt}\right| \Big/ \dot{\varepsilon}_g \lambda \leq 1 \tag{6}$$

where, $\dot{\varepsilon}_g = \max\left|eigenvalue\left(\boldsymbol{d}\right)\right|$ is the strain rate of the flow. The above inequality represents, in a sense, the fraction of $l_{\max}$ not at equilibrium, at each stage of deformation. This leads to the following equation for the effective maximum contour length ratio

$$\lambda_{\text{eff}} = \left[1 - \frac{1}{\dot{\varepsilon}_g \lambda}\left|\frac{d\lambda}{dt}\right|\right](\lambda_{\max} - 1) + 1. \tag{7}$$

Equation 7 describes the coarse-grained internal conformation of the polymer chain molecule in strong extensional flows by allowing a variation of the maximum contour length ratio of the chain segment at each stage of deformation. This equation contains a stretch term, $\dot{\varepsilon}_g\lambda$, which leads to affine stretching of the polymer chain due to hydrodynamic drag. A second term, $\left|\frac{d\lambda}{dt}\right|$, governs the instantaneous stretch ratio dynamic, which is controlled by the Rouse time, τ_{R}.

In order for the model to always represent a polymer chain or a subchain of the same fixed maximum contour length ratio, $\lambda_{\max}$, we introduce the number of "subsegments" defined as follows

$$M_{\text{s}} = \frac{\lambda_{\max}}{\lambda_{\text{eff}}}. \tag{8}$$

We further assume a simplified situation where all chain segments behave in the same way, i.e., the orientation and lengths of all segments are identical. Therefore, the stress contribution of one segment must be multiplied by the number of subsegments to give the contribution of the macromolecules to the stress. Then, Eq. 4 generalizes to

$$\boldsymbol{\tau}_{\text{p}} = M_{\text{s}} G k_{\text{s}}(\lambda)(\boldsymbol{\sigma} - \boldsymbol{I}) = M_{\text{s}} \frac{\eta_{\text{p}}}{\tau_{\text{d}}} k_{\text{s}}(\lambda)(\boldsymbol{\sigma} - \boldsymbol{I}). \tag{9}$$

Matrix-logarithm of the conformation tensor

In order to address complex flows of linear entangled polymers, we use an approach that combines the matrix-logarithm-based formulation of the conformation tensor as proposed by Fattal and Kupferman (2004) and the stabilized discrete elastic viscous stress-splitting method (Guénette and Fortin 1995).

It is known that catastrophic breakdown of viscoelastic problems may be caused by the failure of polynomial-based approximations to properly represent exponential profiles developed by the conformation tensor near stagnation points or in regions of high deformation rate. Fattal and Kupferman (2004) resolved that difficulty through the transformation of differential constitutive models into an equation for the matrix logarithm of the conformation tensor, which we now derive in the general context of the Rolie-Poly model with finite extensibility.

To derive the evolution equation for the logarithm of the conformation tensor $\boldsymbol{\sigma}$, which we denote, $\boldsymbol{\psi} = \log \boldsymbol{\sigma}$, we follow the method of Hulsen et al. (2005) based on the evolution of the principal axes of the deformation tensor and derive the equations in the tensorial form. The diagonalizing transformation of the conformation tensor, $\boldsymbol{\sigma}$, can be written as

$$\boldsymbol{\sigma} = \boldsymbol{R}\tilde{\boldsymbol{\sigma}}\boldsymbol{R}^{\text{T}} = \boldsymbol{R}\begin{pmatrix} \tilde{\sigma}_{11} & 0 & 0 \\ 0 & \tilde{\sigma}_{22} & 0 \\ 0 & 0 & \tilde{\sigma}_{33} \end{pmatrix}\boldsymbol{R}^{\text{T}} \tag{10}$$

Here, $\tilde{\boldsymbol{\sigma}}$ is a diagonal matrix whose diagonal elements, $\tilde{\sigma}_{\text{kk}}$, are eigenvalues of $\boldsymbol{\sigma}$, and $\boldsymbol{R}$ is an orthogonal tensor whose columns are eigenvectors of $\boldsymbol{\sigma}$. The matrix logarithm of the conformation tensor can then be written as

$$\boldsymbol{\psi} = \log \boldsymbol{\sigma} = \boldsymbol{R}(\log \tilde{\boldsymbol{\sigma}})\boldsymbol{R}^{\text{T}}, \tag{11}$$

from which we derive (after some manipulations) the evolution equation for the matrix logarithm of the conformation tensor, $\boldsymbol{\psi}$, in the following form

$$\dot{\psi}_{ij} = R_{ik}\tilde{N}_{km}R_{jm}. \tag{12}$$

The diagonal and off-diagonal components of the tensor $\tilde{N}$ are defined, respectively, as

$$\tilde{N}_{mm} = 2\tilde{L}_{mm} + \tilde{\sigma}_{mm}^{-1}\tilde{f}_{mm}, \tag{13}$$

and

$$\tilde{N}_{km} = \frac{\log\tilde{\sigma}_{mm} - \log\tilde{\sigma}_{kk}}{(\tilde{\sigma}_{mm} - \tilde{\sigma}_{kk})} \times \left[\left(\tilde{L}_{km}\tilde{\sigma}_{mm} + \tilde{L}_{mk}\tilde{\sigma}_{kk}\right)\right], \text{ with } k \neq m. \tag{14}$$

In the limit that $\tilde{\sigma}_{mm} \to \tilde{\sigma}_{kk}$, we get from Eq. 14

$$\tilde{N}_{km} = \left(\tilde{L}_{km} + \tilde{L}_{mk}\right), \text{ with } k \neq m. \tag{15}$$

Finally, the equations governing the conservation of mass and transport of momentum are, for viscoelastic incompressible flow,

$$\nabla \cdot \boldsymbol{u} = 0, \tag{16}$$

$$-\nabla p + \nabla \cdot \left(2\eta_s \boldsymbol{d} + \boldsymbol{\tau}_p\right) = \rho\left[\frac{\partial \boldsymbol{u}}{\partial t} + (\boldsymbol{u} \cdot \nabla)\,\boldsymbol{u}\right] \tag{17}$$

Here, $\boldsymbol{u}$ is the fluid velocity, ρ the fluid density, and p the hydrodynamic pressure. The extra stress tensor has been split into a polymeric contribution $\boldsymbol{\tau}_p$ and a solvent contribution with η_s the solvent viscosity, and $\boldsymbol{d}$ is the rate-of-deformation tensor.

At each time step, the resolution of the full model is performed in a decoupled fashion using an iterative scheme. The momentum and the continuity equations are first solved as a saddle-point problem, with the viscoelastic stress treated as a given body force. The constitutive equation is then integrated with known kinematics. Implicit Euler approximation to the time derivative in the momentum and constitutive equations is used. A fixed-point algorithm is used to iterate between the solution of the momentum and constitutive equations at each time step, thereby making the overall algorithm coupled in a segregated manner. The stabilized discrete elastic viscous stress splitting method (Guénette and Fortin 1995), the streamline upwind Petrov–Galerkin technique as developed by Carew et al. (1993), and the stabilized GLS (Ilinca et al. 2000; Bonvin et al. 2001) are used to carry out three-dimensional time-dependent simulations. Such stabilized methods allow the use of velocity and pressure interpolants that do not satisfy the Babuska–Brezzi condition such as the linear equal order interpolation functions. These elements are both computationally effective and easy to implement, especially for three-dimensional applications. The resulting formulation is well posed. Computations are conducted using our parallel computation framework.

Finally, the methodology used in the present work can be summarized in the following algorithm at a given discrete time t_n:

- Step 1: The viscoelastic stress $\boldsymbol{\tau}_p$ being given, solve the momentum and the mass balance equations for the velocity $\boldsymbol{u}$ and pressure p using the Euler implicit scheme.
- Step 2: Get the rate-of deformation tensor $\boldsymbol{d}$ from $\boldsymbol{u}$ by the least squares method.
- Step 3: The velocity $\boldsymbol{u}$ and the rate-of-deformation tensor $\boldsymbol{d}$ being given, solve the viscoelastic equation, for the matrix logarithm tensor $\boldsymbol{\psi}$, using the Euler implicit scheme.
- Step 4: Get the conformation tensor $\boldsymbol{\sigma}$ from $\boldsymbol{\sigma} = \exp(\boldsymbol{\psi}) = \boldsymbol{R}\left[\exp\left(\tilde{\boldsymbol{\psi}}\right)\right]\boldsymbol{R}^{\mathrm{T}}$;
- Step 5: Get the viscoelastic stress $\boldsymbol{\tau}_p$ from $\boldsymbol{\tau}_p = M_s \frac{\eta_p}{\tau_d} k_s(\lambda)(\boldsymbol{\sigma} - \boldsymbol{I})$.
- Step 6: Check $\boldsymbol{u}$ and $\boldsymbol{\tau}_p$ for convergence of the full problem at the current time t_n and return to step 1 if necessary.

The practical utility and effectiveness of the proposed numerical scheme is demonstrated by solving a fully three-dimensional constriction flow.

Simple shear and uniaxial extensional flows

A systematic comparison of the extended Rolie-Poly model with experimental data has been documented by Kabanemi and Hétu (2009). Here, we only briefly show some selected results that demonstrate its predictive capabilities in shear and uniaxial extensional flows. We further include in these comparisons results of the MLD model and the experimental data from Ye et al. (2003). We refer the reader to the literature cited above for a thorough discussion on experimental and numerical validation of the model. The polymer used in this study is a nearly monodisperse linear polystyrene sample L289 (Ye et al. 2003). The following fluid parameters are used in the model: $\eta_p = 1{,}643.12$ Pa s, $\tau_d = 9.4$ s, $\tau_R = 0.76$ s, $\beta = 0.1$, and $\delta = -0.5$. The fixed maximum stretch ratio was adjusted arbitrarily to $\lambda_{max} = 10$. The steady state curves of the extensional stress are shown in Fig. 1. We further add in this figure predictions using a different value of the extensibility parameter of $\lambda_{max} = 4.5$. At low strain rate for which

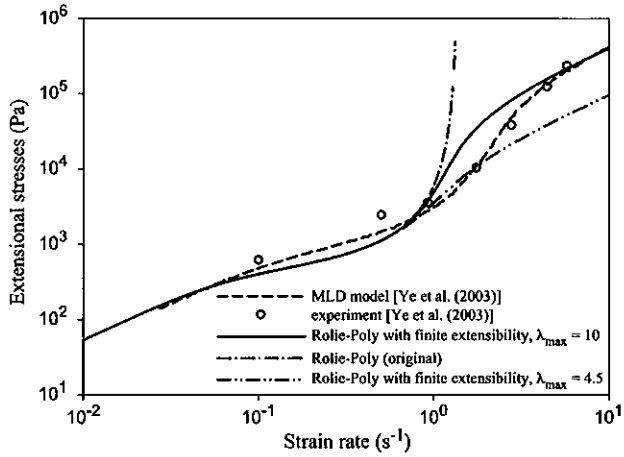

Fig. 1 Steady-state extensional stress prediction compared to that of the original Rolie-Poly model, the MLD model [Ye et al. (2003)] and the experimental data for a nearly monodisperse linear polystyrene sample (L289) [Ye et al. (2003)]

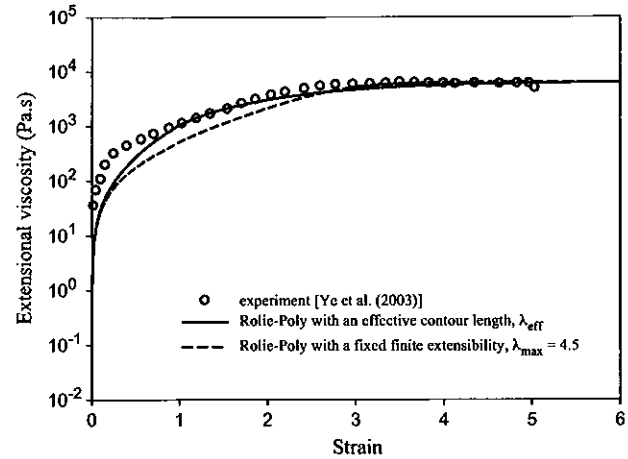

Fig. 2 Prediction of the transient extensional viscosity for the Rolie-Poly model with a fixed finite extensibility, λ_{max}, and with an effective maximum contour length, λ_{eff}, compared to the experimental data for a nearly monodisperse linear polystyrene sample (L289) [Ye et al. (2003)] at strain rate of $\dot{\varepsilon} = 2\ s^{-1}$

$\dot{\varepsilon}\tau_R \leq 1$, predictions are in good agreement with experimental data. In the stretching regime for which $\dot{\varepsilon}\tau_R > 1$, however, predictions become sensitive to the value of the maximum stretch ratio, and the original Rolie-Poly model fails since it omits chain finite extensibility effects. The extensional stress is predicted to be linear in the rate of deformation at high $\dot{\varepsilon}\tau_R$, for both the MLD model and the extended Rolie-Poly model. We would like to point out that, even with the extended Rolie-Poly model, quantitative agreement with experimental data is hardly achieved due to the simplification of single segment model, in which all chain segments are assumed to behave in the same way.

In Fig. 2, we compare the prediction of the transient extensional viscosity, in start-up of uniaxial extensional flow to the experimental data for the same polystyrene from Ye et al. While the steady-state predictions are in agreement with the experimental data, the predicted stress growth at small strain, using the Rolie-Poly model with a fixed maximum contour length ratio, λ_{max}, is slower than the one measured experimentally. The extended model with an effective contour length ratio, λ_{eff}, correctly predicts the stress growth at small strain. This behavior is connected to special conformations of the polymer chains (kinked conformations between entanglement points) that build up during strong extensional flows.

Figure 3 shows the steady shear viscosity as predicted with the current model. We further include in Fig. 3 experimental data from Ye et al. for comparison. While the current model gives good prediction at small shear rates, it underpredicts the steady shear viscosity at high shear rates.

Summarizing the rheological predictions (see also Kabanemi and Hétu 2009), we may conclude that the Rolie-Poly model with an effective maximum contour length ratio, λ_{eff}, is significantly better than the original Rolie-Poly model which does not include finite extensibility and therefore can be used to interpret future simulations of nonequilibrium complex flows. We turn next to this issue.

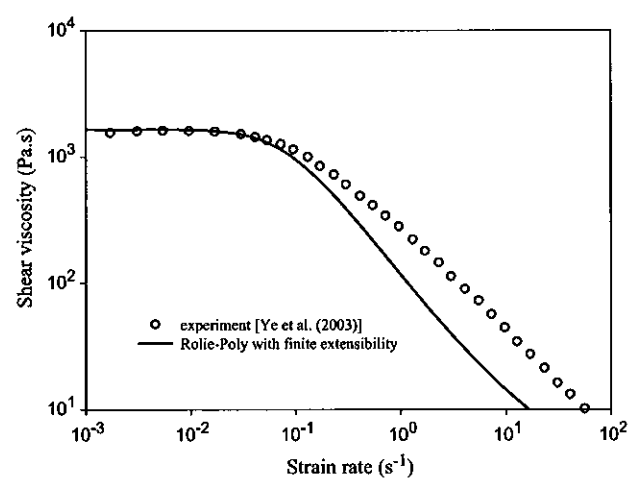

Fig. 3 Steady-state shear viscosity for the Rolie-Poly model with finite extensibility, $\lambda_{max} = 10$, compared to the experimental data for a nearly monodisperse linear polystyrene sample (L289) [Ye et al. (2003)]

Start-up of flow through an axisymmetric 4:1:4 constriction

In this section, we investigate the predictive capabilities of the extended Rolie-Poly model, with an emphasis on polymer conformational changes during the startup of flow through an axisymmetric 4:1:4 constriction. A sketch of the three-dimensional 4:1:4 constriction geometry is given in Fig. 4. The whole three-dimensional domain is used for computations, with the objective of capturing a possible transition to a three-dimensional flow. In order to achieve a fully developed flow upstream and downstream of the constriction, we take an inlet length of $L_u = 80$ mm and an outlet length of $L_d = 160$ mm, while the constriction length is $L_c = 3.175$ mm. The radius of the cylindrical tubes upstream and down stream of the constriction is $R_1 = 12.7$ mm, while the radius of the constriction tube is $R_c = 3.175$ mm. We consider the limit that the Reynolds number is negligible, while $\eta_s = 0$. Starting from rest and using time-independent (static) inlet boundary conditions, we obtained results through a true three-dimensional transient development. We are therefore able to capture possible flow bifurcations and all the important three-dimensional flow features in different flow regimes. The fluid parameters are those of the nearly monodisperse polystyrene solution L289, used in the preceding section. The fixed maximum stretch ratio was reduced to 5. The choice of a small value was made in order to mimic dissipative stress after only a small degree of stretch.

We first analyze the results for the Rolie-Poly model with a fixed maximum contour length ratio, λ_{max}. The Weissenberg number, Wi, based on the Rouse relaxation time for this problem, is defined by $Wi = \tau_R \langle u_z \rangle / R_c$ where $\langle u_z \rangle = Q/\pi R_c^2$ is the average axial velocity in the constriction tube and Q is the volume flow rate. The flow rate is 170π mm^3/s, which corresponds to a Weissenberg number, $Wi = 4.03$. This is large enough to reach the stretch-dominated flow regime in the constriction region. Let us now consider how steady state is established starting from equilibrium initial conformation, $\boldsymbol{\sigma} = \boldsymbol{I}$.

The first global quantity we analyze is the chain stretching evolution during start-up, i.e., the chain conformational changes. Figures 5a–c shows the temporal evolution of the stretch along the axis of symmetry ($r = 0$), along the $r = 2.9$ mm line, i.e., near the wall of the constriction tube and along the radial direction at $z = -0.1$ mm, i.e., in the entry section to the constriction tube, respectively. From these figures, we observe that the chain extensional ratio exhibits a maximum in the entry section to the constriction tube and in the small tube. We further observe that, after only a relatively short time ($t = 0.3$ s), the polymer chains are already stretched in theses two regions. The largest predicted steady stretch ratio is about 3.5. As can be seen from Fig. 5b, the overshoot in the chain stretch is clearly exhibited in the constriction tube, as a result of the strong shear flow present in this region. The average shear rate in the constriction tube is $\dot{\gamma} = \langle u_z \rangle / R_c = 5.3\ \mathrm{s}^{-1}$. We also observe from Fig. 5a, b that the equilibrium stretch ratio becomes smaller than unity downstream of the constriction, as a result of biaxial extension and relaxation. Whether this result is physically realistic is open to discussion. However, one should keep in mind

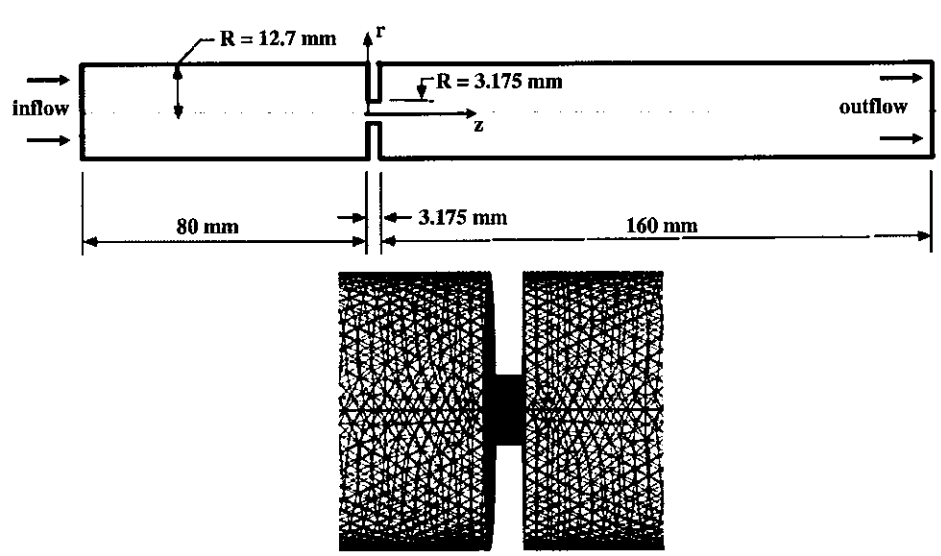

Fig. 4 The geometry and a zoom of the three-dimensional mesh for the 4:1:4 axisymmetric constriction problem. The full grid extends between $z = -80$ mm and $z = 163.175$ mm. The constriction length is $L_c = 3.175$ mm. Upstream re-entrant corners are defined by $z = 0$ and $r = \pm 3.175$ mm. Flow is from left to right

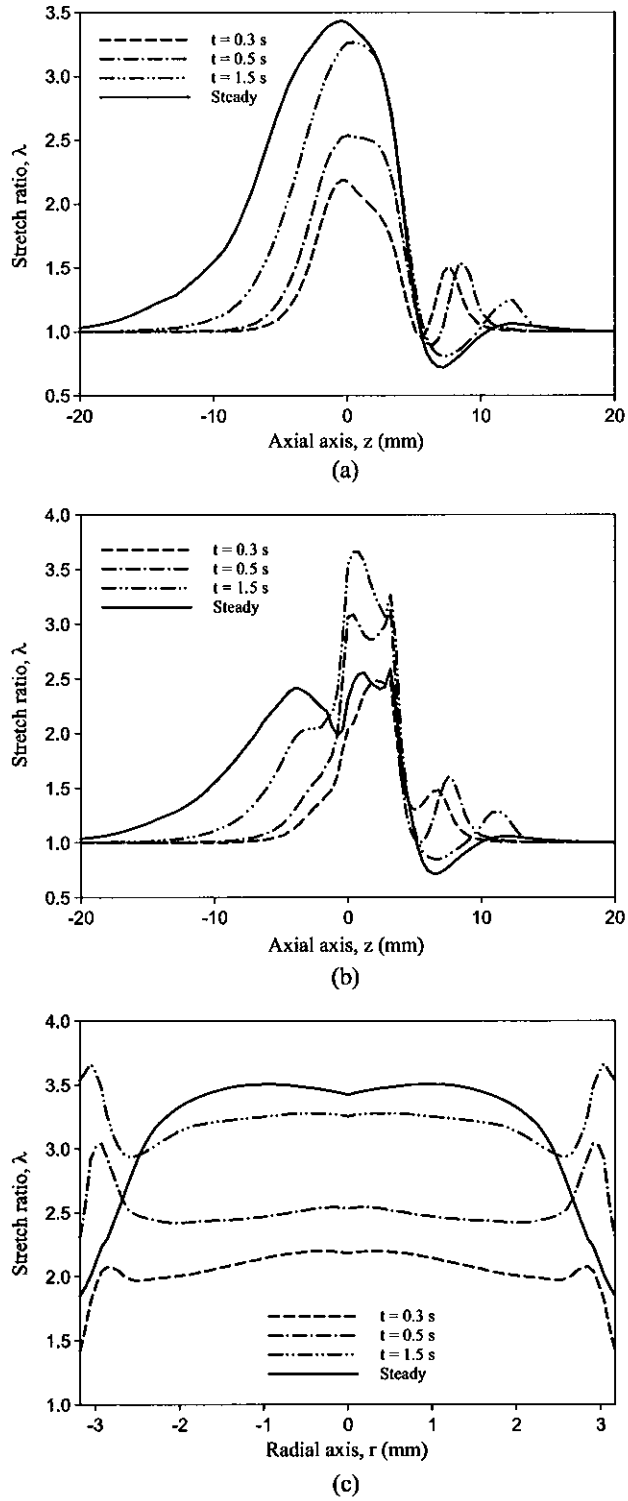

Fig. 5 Transient and steady-state stretch ratio during the start-up of flow through an axisymmetric 4:1:4 constriction, at $Wi = 4.03$: **a** along the center line ($r=0$); **b** along the $r=2.9$ mm line, that is, near the wall of the constriction tube; and **c** along the radial direction at $z=-0.1$ mm, that is, in the entry section to the constriction tube. According to Fig. 4, $z=0$ corresponds to the upstream re-entrant corner, while $r=\pm 3.175$ mm corresponds to wall of the constriction tube

that the original Rolie-Poly model contains a retraction term, which corresponds to relaxation to zero. It is also pertinent to note from Fig. 5c that polymer chains experience a larger transient stretch near the upstream re-entrant corners than the corresponding steady-state stretch ratio. This behavior corresponds to the transient overshoot exhibited by chain segments in that region. In Fig. 6, we display the vortex growth in the middle plane ($r = 0$) during the start-up of flow. We also show in the same figure transients of the stretch field. There is a clear evidence of a lip vortex growth as displayed in Fig. 6, at $t = 0.3$ and 0.5 s, stretching from re-entrant corners. Chain stretching as a function of Wi is shown in Fig. 7a–c. The maximum stretched conformation is reached in the entry section to the constriction tube.

The second important global quantity is the pressure drop in the axisymmetric tube due to the constriction. Considering the large CPU time needed to complete a full three-dimensional transient calculation, only three flow rates are considered. Following Wapperom and Keunings (2001), we define a dimensionless pressure drop in the constriction as $\delta p = (\Delta p - \Delta p^0)/\Delta p^0$, where Δp is the total pressure drop in the flow domain and Δp^0 corresponds to fully developed Poiseuille flow in a tube without constriction, i.e., of length 243.175 mm and radius 12.7 mm. The pressure drop variation as a

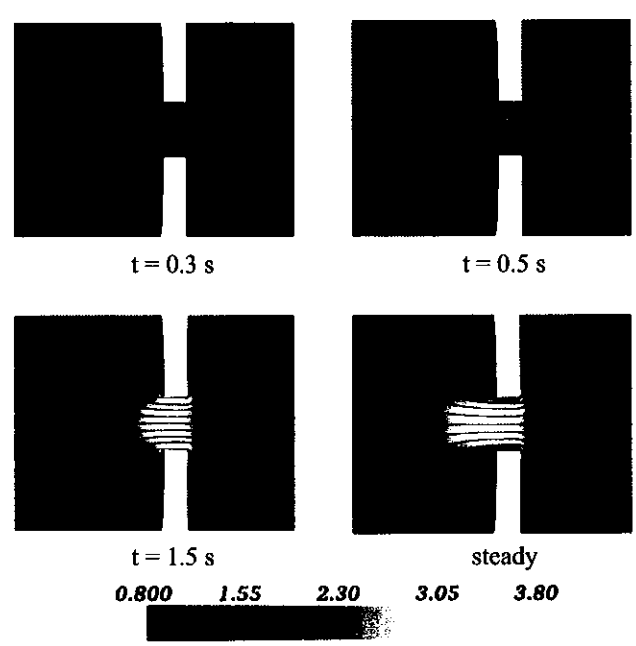

Fig. 6 Temporal evolution of the stretch ratio and vortex growth in the middle plane ($r = 0$) during the start-up of flow through an axisymmetric 4:1:4 constriction at $Wi = 4.03$. Flow is from left to right

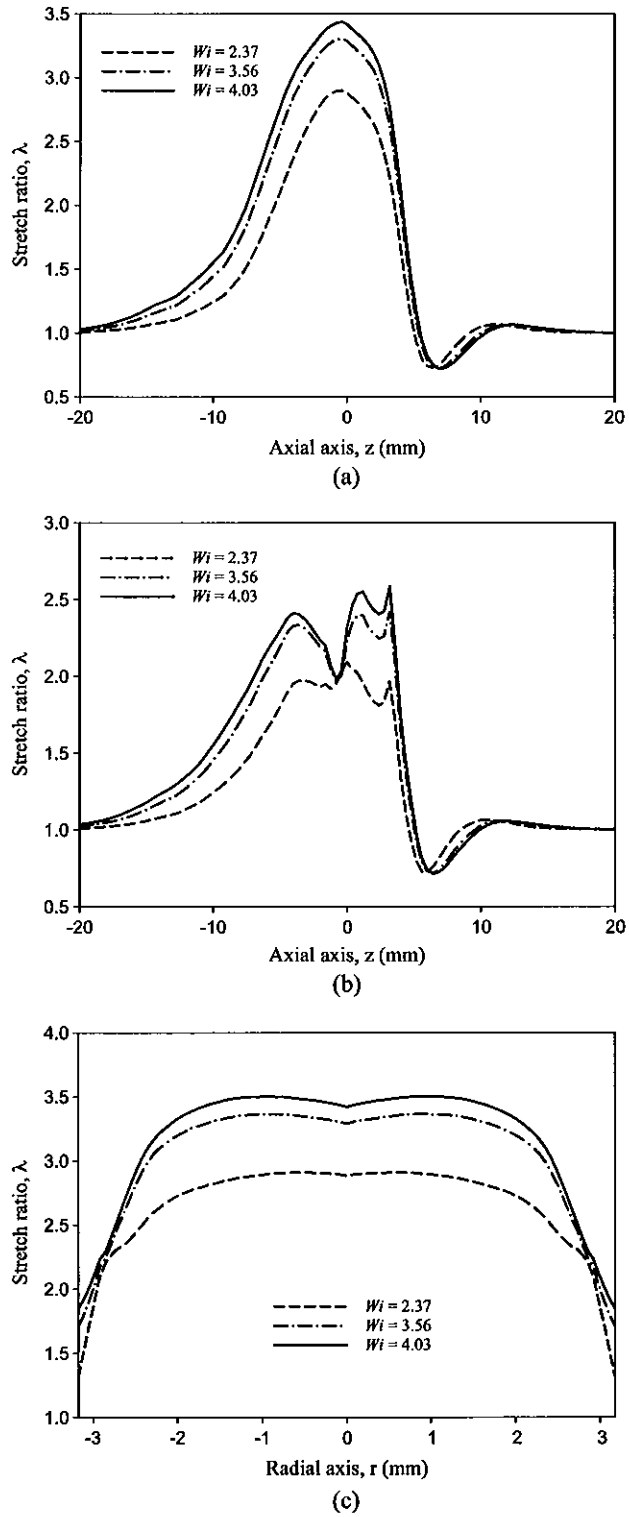

◀ **Fig. 7** Steady-state stretch ratio as a function of the Weissenberg numbers, $Wi = \tau_R \langle u_z \rangle / R_c$, in the start-up of flow through an axisymmetric 4:1:4 constriction: **a** along the center line ($r = 0$); **b** along the $r = 2.9$ mm line, that is, near the wall of the constriction tube; and **c** along the radial direction at $z = -0.1$ *mm*, that is, in the entry section to the constriction tube. According to Fig. 4, $z = 0$ corresponds to the upstream re-entrant corner while $r = \pm 3.175$ mm corresponds to wall of the constriction tube

function of *Wi* is shown in Fig. 8. Contrary to reptation-based models such as DCR model or Pompom model (Wapperom and Keunings 2001; Wapperom et al. 2003) which predict a decrease in the dimensionless pressure drop, the Rolie-Poly model, with a finite extensibility λ_{max} included, predicts an increase in the dimensionless pressure drop with *Wi*. Such results demonstrate that the predicted extra pressure drop is not a result of the stress-conformational hysteresis alone, as we are using the modified model with a fixed maximum contour length that does not predict hysteretic behavior. It is also a consequence of the elastic stress growth due to chain resistance to stretching arising from the finite extensibility included in the model that mimics dissipative stress.

In order to examine the consequence, in a complex flow, of stress-conformation hysteresis on chain conformational changes and flow dynamics, let us consider the flow of the extended Rolie-Poly model with an effective maximum contour length, λ_{eff}. Figure 9 shows the transient total pressure drop in the flow domain, $\Delta p = p_{in} - p_{out}$, at $Wi = 3.56$, up to $t = 1.3$ s. In the same figure, we also show the transient total pressure drop, Δp, using the Rolie-Poly model with a fixed maximum contour length, λ_{max}. The model with λ_{eff} predicts a rapid rise of the pressure drop at the inception of

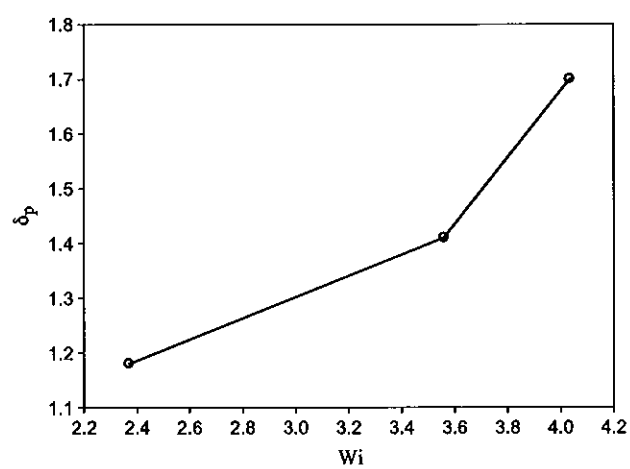

Fig. 8 Dimensionless pressure drop, δp, as a function of Weissenberg number, $Wi = \tau_R \langle u_z \rangle / R_c$, during the flow through an axisymmetric 4:1:4 constriction

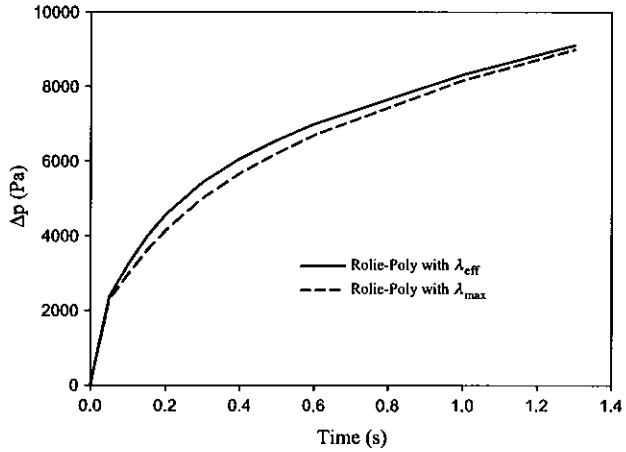

Fig. 9 Transient total pressure drop, $\Delta p = p_{in} - p_{out}$, at $Wi = 3.56$, during the flow start-up through an axisymmetric 4:1:4 constriction, at the inception of the flow

flow as a result of an additional polymeric stress arising from the stress-conformation hysteresis. Figure 10 shows the transient average internal structure of the polymer chain, i.e., the effective maximum contour length ratio in the middle plane ($r = 0$). Chain segments along the flow centerline, in the entry section to the constriction tube, are stretched with a shorter effective maximum contour length at the inception of flow, as highlighted in Fig. 10. This directly suggests that the chain segment is driven into a highly kinked internal configuration state, at these early stages of the flow. We observe that kinked configurations within chain segments are exhibited near the upstream contraction plane, prior to the development of upstream vortices. This behavior results in an additional increase in the transient total pressure drop compared to the results with a fixed maximum contour length, λ_{max} (see Fig. 9). We further observe that kinked configurations within chain segments appear to persist for a long moment near re-entrant corner regions and in the converging flow region, reflecting that in these regions polymer chains are stretched with a shorter λ_{eff} compared to λ_{max} for a long time, before the steady state regime is reached. Figure 11 shows the flow structures in the middle plane ($r = 0$), using the two models, based on the fixed and the effective maximum contour lengths.

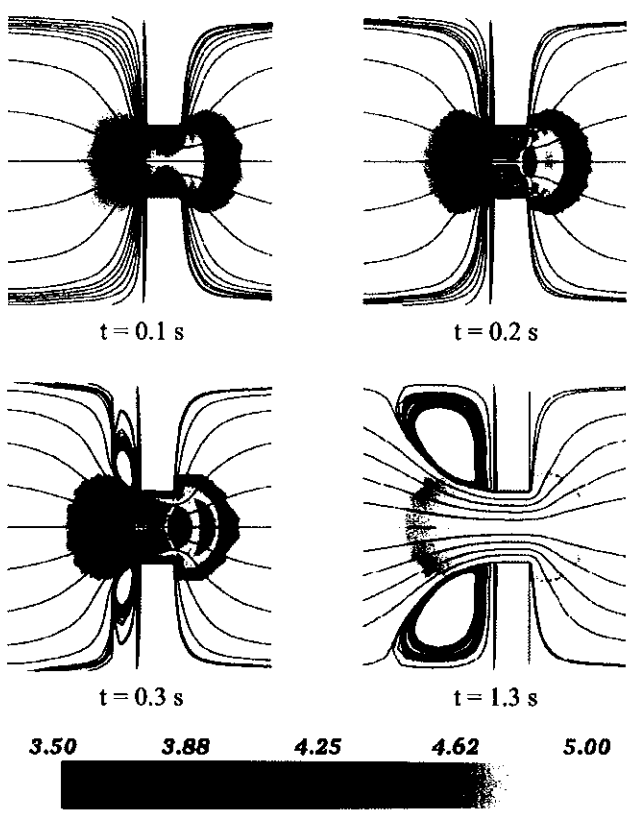

Fig. 10 Temporal evolution of the effective maximum contour length ratio, λ_{eff}, and vortex growth in the middle plane ($r = 0$) during the start-up of flow through an axisymmetric 4:1:4 constriction, at $Wi = 3.56$. Flow is from left to right

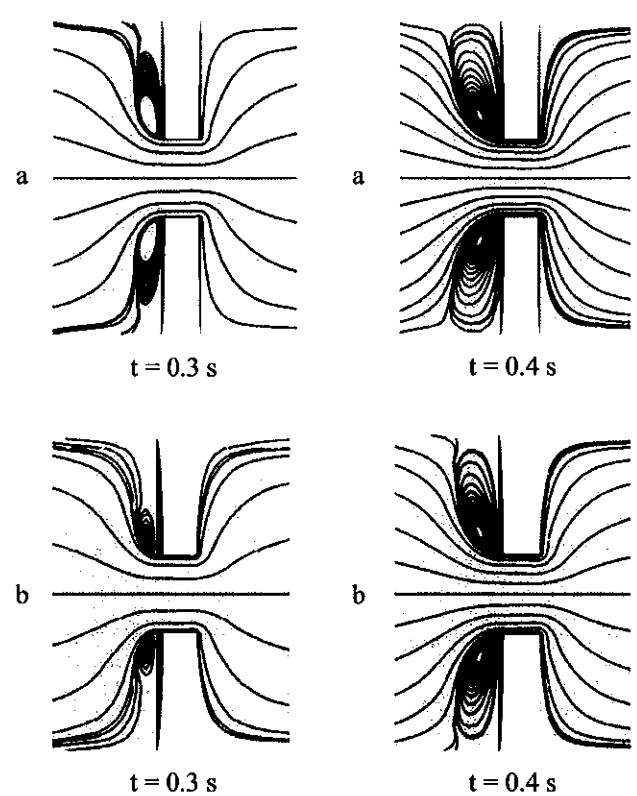

Fig. 11 Vortex growth in the middle plane ($r = 0$) during the start-up of flow at two different times and at $Wi = 3.56$. Rolie-Poly model: **a** with the effective maximum contour length and **b** with the fixed maximum contour length. Flow is from left to right

A noticeable difference in the vortex growth patterns, soon at the inception of flow, is predicted. A lip vortex enhancement is evident right up to the inception of the flow start-up as a consequence of the additional polymeric stress.

Finally, here are a few comments about the ability of the extended Rolie-Poly model, combined with a fully three-dimensional time-dependent finite element method for calculating flow transitions in complex flow problems without performing a linear stability analysis or a weakly nonlinear analysis.

We note from the above predictions, based on a time-dependent three-dimensional finite element method, that while the extended Rolie-Poly model is able to predict the excess pressure drop resulting from the additional polymeric stress or stress-conformation hysteresis, the three-dimensional flow patterns did not reveal any anomalies that could be connected with the onset of instability in the upstream converging flow, at least over the range the flow rate investigated. Nevertheless, kinked configurations within chain segments are predicted in the entry section to the constriction tube, at the inception of the flow. As a result, polymer chains are forced to stretch with a shorter effective maximum contour length, leading to additional polymeric stress, which is reflected in the enhancement of the pressure drop. Unfortunately, the predicted upstream flow keeps a stable axisymmetric mean structure, as highlighted in Fig. 6. We want to emphasize here that, contrary to the extended model used in the present work, the original Rolie-Poly model does not have finite extensibility included, which would limit the degree of strain hardening in the stretching flow regime. Therefore, artificial instabilities may be predicted with the original Rolie-Poly model in fast flows, when non-Gaussian behavior cannot be ignored. The onset of instabilities reported by Collis et al. (2005) for a planar constriction flow, but not documented, should be an artifact of the model. Indeed, the original Rolie-Poly model does not have steady-state extensional viscosity for $Wi \geq 1$, when chains stretch significantly (see Fig. 1).

It is well known that transient finite-element calculations can be used to detect the onset of true physical instabilities. Indeed, Northey et al. (1992) used successfully nonlinear time-dependent simulations to demonstrate the existence of supercritical, time-periodic flow states that evolve as Hopf bifurcation in axisymmetric Taylor-Couette flow between parallel cylinders. Sureshkumar et al. (1999) studied the influence of nonlinear interactions on the dynamics of both the plane Couette flow and the flow through a periodic array of cylinders by using time-dependent simulations based on the DEVSS-G/SUPG/θ-method. In their nonlinear calculations, the initial condition was constructed by superimposing the linear eigenmode, obtained from long-time integration of the linearized equations, onto the steady-state solution for a particular value of *De*. On the other hand, Atalik and Keunings (2002) and Meulenbroek et al. (2004) conducted a nonlinear stability analysis for Poiseuille flow of viscoelastic fluids (UCM, Oldroyd-B, and Giesekus models) between plates and through a tube and confirmed a scenario in which Poiseuille flow of viscoelastic fluids exhibits a nonlinear subcritical instability due to normal stress effects. Even though the existence of a special region as the die entry has not been considered in their work, Meulenbroeck et al. suggested that this nonlinear instability could be an important intrinsic route to melt fracture behavior in the absence of other mechanisms such as stick-slip phenomena. Whether this predicted instability originates from real physical mechanisms is questionable. In fact, Wang (1999), in reviewing results on capillary flow instabilities, pointed out that theoretical effort generally takes the viewpoint that any model capable of producing unstable flow may offer an explanation for real flow instabilities. Both the linear stability analysis and the nonlinear simulations assume that the flow exhibits spatial periodicity, and it is not clear whether or not it holds true also for problems without periodic boundary conditions. Indeed, Bodart and Crochet (1993) considered the flow of an Oldroyd-B fluid through a four-to-one contraction and used a full implicit time-dependent two-dimensional finite element method with the objective of predicting a possible Hopf bifurcation in entry flows observed by Lawler et al. (1986) and McKinley et al. (1991). Starting from a steady state, they imposed a pressure impulse in the entry section, without periodic boundary conditions, and calculated the approach toward another steady state. Unfortunately, they did not observe flow transitions in their calculations.

We too, armed with more advanced constitutive models for linear entangled polymers that capture the essence of physics involved in these flow problems, along with a fully three-dimensional time-dependent finite element method, have not observed the onset of true physical instabilities. This raises the question of true mechanisms that govern instabilities in entry flows of viscoelastic fluids. Ongoing work is carried out in this direction.

Conclusion

We have here used the extended Rouse-CCR tube model for linear entangled polymers recently proposed

by Kabanemi and Hétu (2009), to analyze, by means of a time-dependent three-dimensional finite element method, the kinematics, pressure drop, and stability of flow through a 4:1:4 constriction in a tube. The resulting model, designed to capture the progressive changes in the average internal structure (kinked state) of the polymer chain, includes an "effective" maximum contour length that depends on local flow dynamics. The model predicts an enhancement of the pressure drop, in the stretch-dominated flow regime, which is also observed experimentally. This excess pressure drop was not associated with the onset of flow instability. In the stretch-dominated flow regime, the model also predicts a rapid rise of the transient total pressure drop at the inception of flow, as chain segments are forced to stretch with a shorter effective maximum contour length, l_{eff}, compared to the original fixed maximum contour length, $l_{\max}$, in the entry section to the constriction tube. Finally, the predicted three-dimensional flow structure did not reveal the onset of flow instability in the upstream converging flow, over the range the flow rate investigated. This raises the question of true mechanisms that govern instabilities in entry flows of viscoelastic fluids.

References

Atalik K, Keunings RK (2002) Non-linear temporal stability analysis of viscoelastic plane channel flows using a fully-spectral method. J Non-Newton Fluid Mech 102:299–319

Bodart Ch, Crochet MJ (1993) Time-dependent numerical simulation of viscoelastic flow and stability. Theor Comput Fluid Dyn 5:57–75

Boger DV, Hur DU, Binnington RJ (1986) Further observations of elastic effects in tubular entry flows. J Non-Newton Fluid Mech 20:31–49

Bonvin J, Picasso M, Stenberg R (2001) GLS and EVSS methods for a three-field Stokes problem arising from viscoelastic flows. Comput Methods Appl Mech Eng 190:3893–3914

Carew EOA, Townsend P, Webster MF (1993) A Taylor–Petrov–Galerkin algorithm for viscoelastic flow. J Non-Newton Fluid Mech 50:253–287

Cartalos U, Piau JM (1992) Creeping flow regimes of low concentration polymer solutions in thick solvents through an orifice die. J Non-Newton Fluid Mech 45:231–285

Collis MW, Lele AK, Mackley MR, Graham RS, Groves DJ, Likhtman AE, Nicholson TM, Harlen OG, Mcleish TCB, Hutchings LR, Fernyhough CM, Young RN (2005) Constriction flows of monodisperse linear entangled polymers: multiscale modeling and flow visualization. J Rheol 49: 501–522

Doyle PS, Shaqfeh ESG, McKinley GH, Spiegelberg SH (1998) Relaxation of dilute polymer solutions following extensional flow. J Non-Newton Fluid Mech 76:79-110

Fattal R, Kupferman R (2004) Constitutive laws for the matrix-logarithm of the conformation tensor. J Non-Newton Fluid Mech 123:281–285

Graham RS, Likhtman AE, McLeish TCB, Milner ST (2003) Microscopic theory of linear, entangled polymer chains under rapid deformation including chain stretch and convective constraint release. J Rheol 47:1171–1200

Guénette R, Fortin M (1995) A new mixed finite element method for computing viscoelastic flows. J Non-Newton Fluid Mech 60:27–52

Hulsen MA, Fattal R, Kupferman R (2005) Flow of viscoelastic fluids past a cylinder at high Weissenberg number: stabilized simulations using matrix logarithms. J Non-Newton Fluid Mech 127:27–39

Ilinca F, Hétu JF, Pelletier D (2000) On stabilized finite element formulations for incompressible advective-diffusive transport and fluid flow problems. Comput Methods Appl Mech Eng 188:235–255

Kabanemi KK, Hétu JF (2009) Nonequilibrium stretching dynamics of dilute and entangled linear polymers in extensional flow. J Non-Newton Fluid Mech 160:113–121

Lawler JV, Muller SJ, Brown RA, Armstrong RC (1986) Laser Doppler velocimetry measurements of velocity fields and transitions in viscoelastic fluids. J Non-Newton Fluid Mech 20:51–92

Li L, Larson RG (2000) Excluded volume effects on the birefringence and stress of dilute polymer solutions in extensional flow. Rheol Acta 39:419–427

Likhtman AE, Graham RS (2003) Simple constitutive equation for linear polymer melts derived from molecular theory: Rolie-Poly equation. J Non-Newton Fluid Mech 114:1–12

Marrucci G (1996) Dynamics of entanglements: a nonlinear model consistent with the Cox-Merz rule. J Non-Newton Fluid Mech 62:279–289

McKinley GH, Raiford WP, Brown RA, Armstrong RC (1991) Nonlinear dynamics of viscoelastic flow in axisymmetric abrupt contractions. J Fluid Mech 223:411–456

Meulenbroek B, Storm C, Morozov AN, van Saarloos W (2004) Weakly nonlinear subcritical instability of viscoelastic Poiseuille flow. J Non-Newton Fluid Mech 116:235–268

Nigen S, Walters K (2002) Viscoelastic contraction flows: comparison of axisymmetric and planar configurations. J Non-Newton Fluid Mech 102:343–359

Northey PJ, Armstrong RC, Brown RA (1992) Finite-amplitude time-periodic states in viscoelastic Taylor–Couette flow described by the UCM model. J Non-Newton Fluid Mech 42:117–139

Pattamaprom C, Driscroll JJ, Larson RG (2000) Nonlinear viscoelastic predictions of uniaxial-extensional viscosities of entangled polymers. Macromol Symp 158:1–13

Piau JM, El Kissi N, Tramblay B (1988) Low Reynolds number flow visualization of linear and branched silicones upstream of orifice dies. J Non-Newton Fluid Mech 30:197–232

Piau JM, El Kissi N, Tramblay B (1990) Influence of upstream instabilities and wall slip on melt fracture and sharkskin phenomena during silicones extrusion through orifice dies. J Non-Newton Fluid Mech 34:145–180

Rothstein JP, McKinley GH (1999) Extensional flow of a polystyrene Boger fluid through a 4:1:4 axisymmetric contraction/expansion. J Non-Newton Fluid Mech 86:61–88

Rothstein JP, McKinley GH (2001) The axisymmetric contraction–expansion: the role of extensional rheology on vortex growth dynamics and the enhanced pressure drop. J Non-Newton Fluid Mech 98:33–63

Rothstein JP, McKinley GH (2002) A comparison of the stress and birefringence growth of dilute, semi-dilute and concentrated polymer solutions in uniaxial extensional flows. J Non-Newton Fluid Mech 108:275–290

Sureshkumar R, Smith MD, Armstrong RC, Brown RA (1999) Linear stability and dynamics of viscoelastic flows using time-dependent numerical simulations. J Non-Newton Fluid Mech 82:57–104

Wang SQ (1999) Molecular transitions and dynamics at polymer/wall interfaces: origins of flow instabilities and wall slip. Adv Polym Sci 138:227–275

Wapperom P, Keunings R (2001) Numerical simulation of branched polymer melts in transient complex flow using pom-pom models. J Non-Newton Fluid Mech 97:267–281

Wapperom P, Keunings R, Ianniruberto G (2003) Prediction of rheometrical and complex flows of entangled linear polymers using the double-convection–reptation model with chain stretch. J Rheol 47:247–265

Ye X, Larson RG, Pattamaprom C, Sridhar T (2003) Extensional properties of monodisperse and bidisperse polystyrene solutions. J Rheol 47:443–468